

## Shrinkage analysis of reinforced concrete floors using shrinkage-adjusted elasticity modulus

F. T. K. Au<sup>†</sup>, C. H. Liu and P. K. K. Lee

*Department of Civil Engineering, The University of Hong Kong  
Pokfulam Road, Hong Kong, P.R. China*

*(Received March 30, 2007, Accepted November 30, 2007)*

**Abstract.** The shrinkage of large reinforced concrete floors often gives rise to cracking problems. To identify the problematic areas, shrinkage movement analysis is often carried out by finite element method with proper creep and shrinkage models using step-by-step time integration. However as the full stress history prior to the time interval considered is necessary, with the increase in the number of time intervals used, the amount of computations increases dramatically. Therefore a new method using the shrinkage-adjusted elasticity modulus (SAEM) is introduced so that analysis can be carried out using one single step. Examples are presented to demonstrate its usefulness.

**Keywords:** age-adjusted elasticity modulus; creep; finite element method; reinforced concrete floor; shrinkage; shrinkage-adjusted elasticity modulus.

---

### 1. Introduction

Shrinkage of a concrete structure as the concrete dries after hardening is a natural phenomenon. It could lead to substantial shortening movement and, if the movement is restrained, serious cracking of the concrete structure. Bažant (2001) recently provided a state-of-the-art review of the prediction of concrete creep and shrinkage. The restraining effects of reinforcement in a concrete structure undergoing shrinkage result in not only axial shortening, but also deflections (Alexander 2002a & 2002b) although the deflections are relatively small compared to those from loading. Various researchers have addressed the important issues of cracking of restrained concrete at early age (Altoubat and Lange 2001) and crack control in restrained reinforced concrete (RC) members (Gilbert 1992, Nejadi and Gilbert 2004).

In many big cities with congested building developments, it is common to have large RC podium structures with several tower blocks on top. In some cases, the shrinkage cracks formed have been causing aesthetic, water leakage and durability problems. The cracking of RC structures is a very complicated phenomenon as it involves the interaction between concrete and steel reinforcement, the shape and size of the structure as well as the stiffness of the supports. A recent parametric study shows that the magnitude of induced stress normally increases with the length of structure and support stiffness (Liu, *et al.* 2006). Such cracking problems can be alleviated by proper planning and analysis of the construction activities (Kim and Cho 2004 & 2005). The development of a systematic approach to the shrinkage movement analysis of RC floors is expected to encourage

---

<sup>†</sup> E-mail: [francis.au@hku.hk](mailto:francis.au@hku.hk)

more practising engineers to spend time on the prevention of problems rather than on remedial works after the problems have surfaced. It helps not only in the identification of problematic areas but also in the decision of a suitable concreting sequence.

The stresses and strains in an RC structure vary with time, during which the shrinkage and creep of concrete gradually develop (Gilbert 1988, Ghali, *et al.* 2002). For the analysis of time-dependent stresses and deformations, it is necessary to utilise the basic time functions for strain or stress of the constituent materials. In the shrinkage analysis of an RC floor comprising beams and slabs supported on columns and walls, the finite element method (Cheung and Yeo 1979, Cook, *et al.* 2002) may be employed taking into account the shrinkage and creep strains induced. As the creep strains within a time interval are dependent on the loading history up to the moment, a step-by-step numerical procedure is normally employed. However if the structure is a complicated one, extensive computer storage is required for the stress history data. The amount of computation also increases drastically as the number of time steps increases to improve accuracy.

To overcome the excessive amount of computation in the step-by-step numerical procedure, approximate methods are commonly used. Trost (1967) proposed a method for evaluating the time-dependent strain due to varying stress under the assumption of concrete with constant elasticity during the period of analysis, and the method was further developed by Dilger and Neville (1971) for analysing time-dependent stresses of reinforced concrete sections. Bažant (1972) modified this method and named it as the age-adjusted effective modulus (AAEM), which is also known as the age-adjusted elasticity modulus (AAEM) (Ghali, *et al.* 2002). The AAEM method hinges on the relaxation function of concrete that is related to the variation of stress due to a unit strain introduced at an instant and kept constant henceforth. The AAEM method assumes that the stress history is a linear algebraic function of the relaxation function and is exact for problems under the special conditions of constant stress or constant strain. This method is widely used because it provides sufficient approximation to many engineering problems.

Although the AAEM method is a very simple approach of linear creep analysis, it cannot give exact solutions to problems of restrained shrinkage in which strains do not vary linearly with the creep coefficient. Therefore a new method using the shrinkage-adjusted elasticity modulus (SAEM) is introduced. The SAEM is derived from the interaction between shrinkage and creep of concrete restrained against movement. Similar to the AAEM method, the new SAEM method reduces the problem to a single step computation thus obviating the need for iterations. The SAEM has been shown to be useful in the shrinkage analysis of RC frames (Au, *et al.* 2007) in which both bending and axial load effects are significant.

Apart from discussing the shrinkage analysis of RC floors by finite element method using the step-by-step numerical procedure, this paper also presents the formulation and validation of the SAEM method. Numerical examples demonstrate that the SAEM method is efficient, versatile and accurate. This paper mainly concentrates on the development of an efficient computational method for evaluation of stresses due to drying shrinkage. Separate analysis should be carried out to obtain the stresses in a structure caused by temperature changes due to either the heat of hydration in the first few days after casting or the subsequent seasonal variations. It should be noted that once cracking initiates causing bond-slip and other phenomena, more involved analysis than the SAEM method is necessary. Nevertheless the SAEM method presents a convenient way for prediction of the general onset of cracking and provides important clues to refinements in the preliminary design to avoid subsequent shrinkage problems.

## 2. Creep and shrinkage of concrete

The time-dependent behaviour of concrete structures can be analysed using a suitable constitutive model of concrete that takes into account creep and shrinkage, and an appropriate algorithm for time integration. This problem has attracted interest of various investigators and is well covered by the literature (Bažant 1982, Bažant 1988, Ghali, *et al.* 2002).

### 2.1. Analytical model for creep and shrinkage of concrete

The total strain  $\varepsilon_c(t)$  at time  $t$ , including the instantaneous and creep strains, due to a constant stress  $\sigma_c(t_0)$  applied at the age  $t_0$  is expressed in terms of the modulus of elasticity  $E_c(t_0)$  at age of loading and the creep coefficient  $\varphi(t, t_0)$  as

$$\varepsilon_c(t) = \frac{\sigma_c(t_0)}{E_c(t_0)} [1 + \varphi(t, t_0)] \quad (1)$$

The calculation of creep caused by time-varying stresses can be determined by the principle of superposition. According to this principle, the strain caused by stress history  $\sigma_c(t)$  is obtained by summation of the responses of  $d\sigma_c(\tau)$  applied at time  $\tau$ . When the magnitude of applied stress changes with time, the total strain of concrete  $\varepsilon_c(t)$  due to the applied stress and shrinkage is given by

$$\varepsilon_c(t) = \sigma_c(t_0) \left[ \frac{1 + \varphi(t, t_0)}{E_c(t_0)} \right] + \int_0^{\Delta \bar{\sigma}_c(t)} \frac{1 + \varphi(t, \tau)}{E_c(\tau)} d\sigma_c(\tau) + \varepsilon_{cs}(t, t_0) \quad (2)$$

where  $\Delta \bar{\sigma}_c(t)$  is the stress increment from time  $t_0$  to  $t$  and  $\varepsilon_{cs}(t, t_0)$  is the free shrinkage from time  $t_0$  to  $t$ . For practical engineering problems, Eq. (2) has to be solved numerically. The entire period of time of interest is divided into time steps of reasonable size for analysis. The finite element method is often used to solve problems of creep and shrinkage involving complicated concrete structures.

As the integral in Eq. (2) involves incremental stress changes over the time steps, for each finite element one must store all preceding values of stress components, and at each time step one must sum up all these stresses. This method is suitable for problems of small to medium size. For larger problems, this method results in extensive storage and computational requirements. As the effects of creep and shrinkage tend to reduce with time, it is acceptable to adopt gradually increasing time steps. One usual strategy is to specify that a step size should bear a constant ratio slightly above unity to its previous step size. Within each time step, the variables are assumed to be varying linearly or remaining constant as appropriate.

### 2.2. Age-adjusted effective modulus (AAEM)

The stress-strain relationship based on the AAEM method offers a very simple approach to linear creep analysis of structure. Bažant (1972) introduced a stress-strain relationship with the assumption that the stress history is a linear algebraic function of the relaxation function. Therefore, the analysis of strain due to gradually introduced stress increment during the period  $(t, t_0)$ , and Eq. (2) is reduced to

$$\varepsilon_c(t) = \sigma_c(t_0) \left[ \frac{1 + \varphi(t, t_0)}{E_c(t_0)} \right] + \Delta \bar{\sigma}_c(t) \frac{1 + \chi_c(t, t_0) \varphi(t, t_0)}{E_c(t_0)} + \varepsilon_{cs}(t, t_0) \quad (3a)$$

$$\bar{E}_c(t, t_o) = \frac{E_c(t_o)}{1 + \chi_c(t, t_o)\varphi(t, t_o)} \quad (3b)$$

where  $\chi_c(t, t_o)$  is the aging coefficient to account for the time-dependent effects due to creep of concrete, and  $\bar{E}_c(t, t_o)$  is the AAEM. This approach permits an estimation of the time-dependent stresses of concrete in a single step, and gives exact solution for creep problems in which the strain varies linearly with the creep coefficient. Nevertheless, Bažant (1972) noted that this method has relatively low accuracy when the strain function is different from the creep function.

### 3. Finite element analysis of the RC floors by step-by-step time integration

In the present shrinkage analysis, the slabs and the beams are modelled by triangular plane stress elements and bar elements respectively. As shrinkage stresses are only significant in large RC floors and the bending effects in such cases are normally secondary in nature, only the in-plane effects are considered here. To include the bending effects, the same approach as in RC frames (Au, *et al.* 2007) can be adopted.

To facilitate subsequent formulation for finite element analysis using the step-by-step time integration (SBSTI), Eq. (2) is rewritten to give the incremental strain  $\Delta\varepsilon_c(t)$  as

$$\Delta\varepsilon_c(t) = \frac{\Delta\sigma_c(t)}{\bar{E}_c(t)} + \Delta\varepsilon_\varphi(t) + \Delta\varepsilon_{cs}(t) \quad (4)$$

where  $\Delta t$  is the time increment and the other component increments are

$$\Delta\sigma_c(t) = \sigma_c(t + \Delta t) - \sigma_c(t) \quad (5a)$$

$$\bar{E}_c(t) = \frac{[E_c(t) + E_c(t + \Delta t)]/2}{1 + \varphi((t + \Delta t, t)/2)} \quad (5b)$$

$$\Delta\varepsilon_\varphi(t) = \frac{\sigma_c(t_o)}{E_c(t_o)}[\varphi(t + \Delta t, t_o) - \varphi(t, t_o)] + \int_{\sigma_c(t_o)}^{\sigma_c(t)} \frac{\varphi(t + \Delta t, \tau) - \varphi(t, \tau)}{E_c(\tau)} d\sigma_c(\tau) \quad (5c)$$

$$\Delta\varepsilon_{cs}(t) = \varepsilon_{cs}(t + \Delta t, t_o) - \varepsilon_{cs}(t, t_o) \quad (5d)$$

The basic idea and formulation of the two-dimensional triangular plane stress element are well established and can be found for instance in Cheung and Yeo (1979). Each node is assumed to have two translational degrees of freedom (Fig. 1(a)). As the stresses and strains are dependent on time, the incremental stress vector  $\Delta\sigma_c$  within a typical time step  $\Delta t$  can be written in terms of the elasticity matrix  $\bar{\mathbf{D}}_c(t)$ , the incremental strain vector  $\Delta\varepsilon_c(t)$  of concrete, the incremental creep strain vector  $\Delta\varepsilon_\varphi(t)$  and the incremental shrinkage strain vector  $\Delta\varepsilon_{cs}(t)$  at time  $t$  as

$$\Delta\sigma_c = \bar{\mathbf{D}}_c(t)(\Delta\varepsilon_c(t) - \Delta\varepsilon_\varphi(t) - \Delta\varepsilon_{cs}(t)) \quad (6a)$$

$$\bar{\mathbf{D}}_c(t) = \frac{\bar{E}_c(t)}{1 - \nu^2} \begin{bmatrix} 1 & \nu & 0 \\ \nu & 1 & 0 \\ 0 & 0 & (1 - \nu)/2 \end{bmatrix} \quad (6b)$$

$$\Delta\varepsilon_c(t) = [\Delta\varepsilon_x(t), \Delta\varepsilon_y(t), \Delta\gamma_{xy}(t)]^T \quad (6c)$$

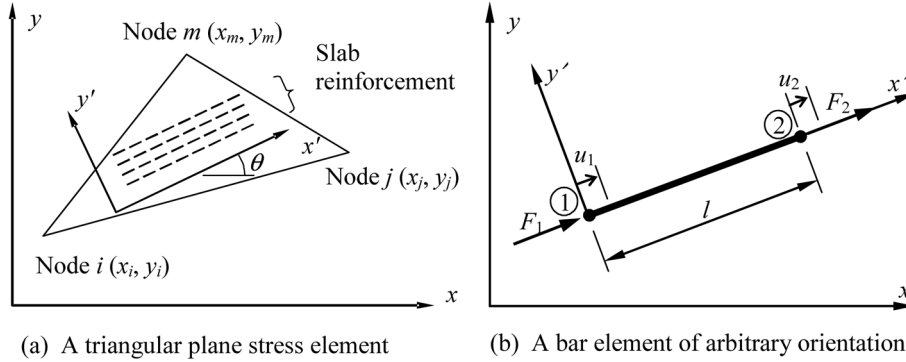


Fig. 1 Triangular plane stress element and bar element for modelling of slab and beam respectively

$$\Delta \boldsymbol{\varepsilon}_\varphi(t) = [\Delta \varepsilon_{\varphi x}(t), \Delta \varepsilon_{\varphi y}(t), \Delta \gamma_{\varphi xy}(t)]^T \quad (6d)$$

$$\Delta \boldsymbol{\varepsilon}_{cs}(t) = [\Delta \varepsilon_{csx}(t), \Delta \varepsilon_{csy}(t), 0]^T \quad (6e)$$

where  $\nu$  is Poisson's ratio;  $\sigma_x$ ,  $\sigma_y$  and  $\tau_{xy}$  are the two direct stresses and shear stress in the  $x$ - $y$  system respectively;  $\varepsilon_{\varphi x}$ ,  $\varepsilon_{\varphi y}$  and  $\gamma_{\varphi xy}$  are the two direct creep strains and shear creep strain in the  $x$ - $y$  system respectively; and  $\varepsilon_{csx}$  and  $\varepsilon_{csy}$  are the two shrinkage strains in the  $x$ - $y$  system respectively. Neglecting body forces and considering incremental quantities, the incremental element nodal force vector  $\Delta \mathbf{q}^e$  can be expressed in terms of the incremental displacement vector  $\Delta \boldsymbol{\delta}$  as

$$\Delta \mathbf{q}^e = \int_{V_e} \mathbf{B}^T \Delta \boldsymbol{\sigma}_c dV = \mathbf{K}_c \Delta \boldsymbol{\delta} - T A \mathbf{B}^T \overline{\mathbf{D}}_c(t) (\Delta \boldsymbol{\varepsilon}_\varphi(t) + \Delta \boldsymbol{\varepsilon}_{cs}(t)) \quad (7)$$

where  $V_e$  is the element volume,  $A$  is the plan area of element,  $\mathbf{B}$  is the strain matrix,  $T$  is the element thickness, and  $\mathbf{K}_c$  is the element stiffness matrix given by

$$\mathbf{K}_c = T A \mathbf{B}^T \overline{\mathbf{D}}_c(t) \mathbf{B} \quad (8)$$

Explicit forms of the above matrices and vectors are given in Appendix A.

The slab is normally provided with several sets of steel reinforcement. As far as the analysis of the effects of shrinkage and creep before the general onset of cracking is concerned, the following assumptions on the steel reinforcement can be made:

- Sufficient steel reinforcement is provided so that it can be assumed to be linearly elastic.
- Each set of steel reinforcement is assumed to be smeared and considered as an orthotropic continuum possessing stiffness in the direction of reinforcement only.
- The concrete and steel reinforcement in the slab are modelled separately. Their interaction within each element is ignored.

The triangular plane stress elements may again be used to model the steel reinforcement. For a typical set of reinforcement shown in Fig. 1(a), the element stiffness matrix is initially formulated with respect to the local  $x'$ - $y'$  coordinate system with the elasticity matrix  $\mathbf{D}'$  taken as

$$\mathbf{D}' = \begin{bmatrix} E_s & 0 & 0 \\ 0 & 0 & 0 \\ 0 & 0 & 0 \end{bmatrix} \quad (9)$$

The element stiffness matrices must be transformed to the global coordinate system (Cook, *et al.*

2002) before assembly.

Bar elements as shown in Fig. 1(b) are used to model the RC beams. The bar elements are assumed to take axial load only. An RC beam segment is modelled by two coincident bar elements to model concrete and steel reinforcement separately. The longitudinal reinforcement is modelled as an elastic bar having the cross sectional area  $A_{sb}$  and modulus of elasticity  $E_s$ . The incremental nodal force vector for the concrete component can be obtained accordingly with respect to the local  $x'-y'$  coordinate system as

$$\begin{Bmatrix} \Delta F_1 \\ \Delta F_2 \end{Bmatrix} = \frac{\bar{E}_c(t)A_b}{l} \begin{bmatrix} 1 & -1 \\ -1 & 1 \end{bmatrix} \begin{Bmatrix} \Delta u_1 \\ \Delta u_2 \end{Bmatrix} + \bar{E}_c(t)A_b \Delta \varepsilon_\phi(t) \begin{Bmatrix} 1 \\ -1 \end{Bmatrix} + \bar{E}_c(t)A_b \Delta \varepsilon_{cs}(t) \begin{Bmatrix} 1 \\ -1 \end{Bmatrix} \quad (10)$$

where  $\Delta F_1$  and  $\Delta F_2$  are the incremental nodal forces at nodes 1 and 2 respectively,  $\Delta u_1$  and  $\Delta u_2$  are the incremental axial displacements at nodes 1 and 2 respectively, and  $A_b$  and  $l$  are the sectional area and length of the concrete component respectively. Before assembling these local matrices and vectors to form the corresponding global matrices and vectors, they must be transformed to the global coordinate system in the usual manner (Cook, *et al.* 2002).

## 4. Shrinkage-adjusted elasticity modulus

### 4.1. Stressing function of concrete due to shrinkage of concrete

When a concrete member is completely fixed at both ends at time  $t_o$ , the shrinkage strain induces tensile stresses as shown in Fig. 2. The variation of shrinkage stress during the period  $(t, t_o)$  can be described by a stressing function that depends on the interaction between shrinkage and creep of concrete. Assuming the initial stress  $\sigma_c(t_o)$  in the concrete member to be zero, Eq. (2) can be simplified in a manner similar to that for AAEM as

$$\varepsilon_c(t) = \Delta \bar{\sigma}_c(t) \frac{1 + \chi_s(t, t_o) \varphi(t, t_o)}{E_c(t_o)} + \varepsilon_{cs}(t, t_o) = 0 \quad (11)$$

where  $\chi_s(t, t_o)$  is the shrinkage coefficient to account for the interaction between creep and shrinkage of concrete. For convenience the stress variation shown in Fig. 2 is described by a shape function  $\xi_1(\tau)$  for  $t \geq \tau \geq t_o$  that is defined as

$$\xi_1(\tau) = \frac{\sigma_c(\tau) - \sigma_c(t_o)}{\sigma_c(t) - \sigma_c(t_o)} = \frac{\sigma_c(\tau)}{\Delta \bar{\sigma}_c(t)} \quad (12)$$

Differentiating Eq. (12) and dropping the dependent variable in  $\xi_1(\tau)$  then gives

$$\frac{d\sigma_c(\tau)}{d\tau} = \Delta \bar{\sigma}_c(t) \frac{d\xi_1}{d\tau} \quad (13)$$

Substituting Eq. (13) into Eq. (2) gives the strain at time  $t$  as

$$\varepsilon_c(t) = \Delta \bar{\sigma}_c(t) \int_{t_o}^t \frac{1 + \varphi(t, \tau) d\xi_1}{E_c(\tau) d\tau} + \varepsilon_{cs}(t, t_o) \quad (14)$$

Comparing Eq. (11) and Eq. (14), the shrinkage coefficient  $\chi_s(t, t_o)$  can be expressed as

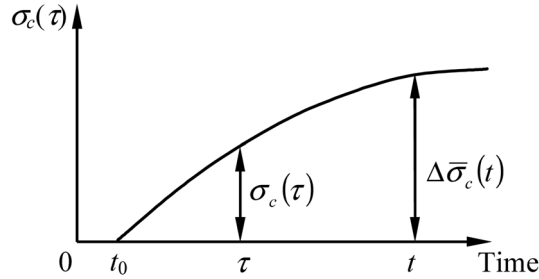


Fig. 2 Development of shrinkage stress in a concrete member fixed at both ends

$$\chi_s(t, t_0) = \frac{E_c(t_0)}{\varphi(t, t_0)} \int_{t_0}^t \frac{1 + \varphi(t, \tau) d\xi_1}{E_c(\tau) d\tau} - \frac{1}{\varphi(t, t_0)} \quad (15)$$

The variation of shrinkage stress or the stressing function  $s(t, t_0)$  under restrained shrinkage condition from time  $t_0$  can be determined by finite element analysis using SBSTI. This is similar in concept to the computed shape function used in finite strip analysis (Cheung and Au 1992) except that the stressing function  $s(t, t_0)$  is a computed shape function in the time domain. Substituting the stressing function  $s(t, t_0)$  as the stress increment  $\Delta \bar{\sigma}_c(t)$  into Eq. (11) and noting that the strain  $\varepsilon_c(t)$  remains zero, the shrinkage coefficient  $\chi_s(t, t_0)$  can be worked out as

$$\chi_s(t, t_0) = -\frac{E_c(t_0) \varepsilon_{cs}(t, t_0)}{s(t, t_0) \varphi(t, t_0)} - \frac{1}{\varphi(t, t_0)} \quad (16)$$

Introducing the shrinkage-adjusted elasticity modulus (SAEM)  $\bar{E}_{cs}(t, t_0)$  for time period  $(t, t_0)$  defined as

$$\bar{E}_{cs}(t, t_0) = \frac{E_c(t_0)}{1 + \chi_s(t, t_0) \varphi(t, t_0)} \quad (17)$$

the stressing function  $s(t, t_0)$  under restrained shrinkage condition from time  $t_0$  can be written in terms of the SAEM  $\bar{E}_{cs}(t, t_0)$  as

$$s(t, t_0) = -\bar{E}_{cs}(t, t_0) \varepsilon_{cs}(t, t_0) \quad (18)$$

As the value of the shrinkage coefficient  $\chi_s$  depends on  $E_c(t_0)$ ,  $\varepsilon_{cs}(t, t_0)$  and  $\varphi(t, t_0)$ , the shrinkage coefficient  $\chi_s(t, t_0)$  and the SAEM  $\bar{E}_{cs}(t, t_0)$  may be calculated and plotted against parameters such as the characteristic concrete strength, effective thickness, relative humidity, etc. Alternatively a subroutine may be written to generate such values using a single bar element when needed.

#### 4.2. Shrinkage with restraint considered in two stages

Large RC structures are often constructed in several stages with concrete cast at different time. The SAEM method can also be modified to account for the effects of construction sequence. Fig. 3 shows the stress development due to shrinkage restrained at time  $t_0$  and  $t_1$  given that curing is stopped at time  $t_0$ . Applying Eq. (18) to different time of restraint  $t_0$  and  $t_1$  where  $t \geq t_1 \geq t_0$  gives the stress difference  $\sigma_d(t)$

$$\sigma_d(t) = s(t, t_0) - s(t, t_1) = -\bar{E}_{cs}(t, t_0) \varepsilon_{cs}(t, t_0) + \bar{E}_{cs}(t, t_1) \varepsilon_{cs}(t, t_1) \quad (19)$$

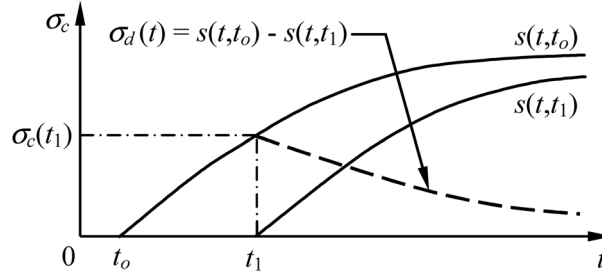


Fig. 3 Shrinkage stress development for restraint introduced at different time

Noting that the shrinkage stress at the end of period  $(t_1, t_0)$  is  $\sigma_c(t_1) = -\bar{E}_{cs}(t_1, t_0)\varepsilon_{cs}(t_1, t_0)$ , the subsequent stress difference  $\sigma_d(t)$  can be written in terms of  $\sigma_c(t_1)$  and the shrinkage-adjusted relaxation function  $\lambda(t, t_1, t_0)$  as

$$\sigma_d(t) = \sigma_c(t_1)\lambda(t, t_1, t_0) \quad (20a)$$

$$\lambda(t, t_1, t_0) = \frac{\bar{E}_{cs}(t, t_0)\varepsilon_{cs}(t, t_0) - \bar{E}_{cs}(t, t_1)\varepsilon_{cs}(t, t_1)}{\bar{E}_{cs}(t_1, t_0)\varepsilon_{cs}(t_1, t_0)} \quad (20b)$$

In summary, the shrinkage stress at any time  $t$  of the concrete member restrained at time  $t_0$  can be written as

$$\sigma_c(t) = -\bar{E}_{cs}(t, t_0)\varepsilon_{cs}(t, t_0) \quad \text{for } t_0 \leq t \leq t_1 \quad (21a)$$

$$\sigma_c(t) = \sigma_c(t_1)\lambda(t, t_1, t_0) - \bar{E}_{cs}(t, t_1)\varepsilon_{cs}(t, t_1) \quad \text{for } t \geq t_1 \quad (21b)$$

Eq. (21b) is written in two components so that it is applicable whether the member is restrained at time  $t_0$  or  $t_1$ . In particular, if the member is free until it is restrained at time  $t_1$ , the shrinkage stress  $\sigma_c(t_1)$  is zero and the equation degenerates to the same form as Eq. (18). This means that for the case of perfect restraints, the solutions obtained should be as accurate as in the SBSTI method to solve for the shrinkage coefficient  $\chi_s(t, t_0)$  and the SAEM  $\bar{E}_{cs}(t, t_0)$ . Defining the stress increment since time  $t_1$  as  $\Delta\sigma_c(t) = \sigma_c(t) - \sigma_c(t_1)$  and the incremental shrinkage strain as  $\Delta\varepsilon_{cs}(t) = \varepsilon_{cs}(t, t_1)$ , for the case of perfect restraints against shrinkage, Eq. (21b) gives

$$\Delta\sigma_c(t) = -\sigma_c(t_1)[1 - \lambda(t, t_1, t_0)] - \bar{E}_{cs}(t, t_1)\Delta\varepsilon_{cs}(t) \quad (22)$$

For cases in which the shrinkage restraints have finite stiffnesses, the development of stresses is expected to follow the same shape function as the case of perfect shrinkage restraints. Analysis is first carried out for the first stage for the time period  $(t_1, t_0)$  to get the stresses at time  $t_1$ , which provide the initial conditions for the analysis of the second stage from time  $t_1$ . Taking into account the incremental strain  $\Delta\varepsilon_c(t)$  since time  $t_1$ , a third term may be added to Eq. (22) giving

$$\Delta\sigma_c(t) = -\sigma_c(t_1)[1 - \lambda(t, t_1, t_0)] - \bar{E}_{cs}(t, t_1)\Delta\varepsilon_{cs}(t) + \bar{E}_{cs}(t, t_1)\Delta\varepsilon_c(t) \quad (22)$$

Eq. (22) can be rearranged to a convenient incremental form similar to Eq. (4) for finite element implementation, namely

$$\Delta\varepsilon_c(t) = \frac{\Delta\sigma_c(t)}{\bar{E}_{cs}(t, t_1)} + \Delta\varepsilon_\lambda(t) + \Delta\varepsilon_{cs}(t) \quad (23a)$$

where the strain caused by initial stress at this stage  $\Delta\varepsilon_i$  is

$$\Delta\varepsilon_i(t) = [1 - \lambda(t, t_1, t_o)] \frac{\sigma_c(t_1)}{\bar{E}_{cs}(t, t_1)} \quad (23b)$$

The above derivation shows that the accuracy of results hinges upon the shrinkage-adjusted relaxation function  $\lambda(t, t_1, t_o)$  that may be generated from the stress variations obtained from a single bar element using Eq. (20b). In addition, it is necessary to verify that  $\lambda(t, t_1, t_o)$  behaves well at the limiting values. It may easily be seen from Eq. (20b) that  $\lambda(t_1, t_1, t_o) = 1$  as  $\varepsilon_{cs}(t_1, t_1)$  vanishes. However  $\lambda(t, t_o, t_o)$  is indeterminate but it may be taken as  $\lambda(t, t_o, t_o) = \lim_{\Delta t \rightarrow 0} \lambda(t, t_o + \Delta t, t_o)$  when time  $t_1$  approaches  $t_o$ . To study the convergence,  $t_o$  is taken as 3 days and the function is evaluated from 3 to 365 days. The increment  $\Delta t$  is varied from  $10^{-4}$  to  $10^{-7}$ . The root mean square value of  $\lambda(t, t_o, t_o)$  from 3 to 365 days remains at 0.601197 throughout the range of  $\Delta t$  thus indicating proper convergence.

### 4.3. Triangular plane stress element using SAEM

Comparing Eq. (23a) in terms of the SAEM with Eq. (4) for the SBSTI method, the incremental stress vector  $\Delta\sigma_c$  can be written similar in form to Eq. (6) in terms of shrinkage-adjusted elasticity matrix  $\bar{\mathbf{D}}_{cs}(t)$ , the incremental strain vector  $\Delta\varepsilon_c(t)$  of concrete, the incremental strain vector  $\Delta\varepsilon_i(t)$  caused by initial stresses and the incremental shrinkage strain vector  $\Delta\varepsilon_{cs}(t)$  at time  $t$  as

$$\Delta\sigma_c = \bar{\mathbf{D}}_{cs}(t, t_1)(\Delta\varepsilon_c(t) - \Delta\varepsilon_i(t) - \Delta\varepsilon_{cs}(t)) \quad (24a)$$

$$\bar{\mathbf{D}}_{cs}(t, t_1) = \frac{\bar{E}_{cs}(t, t_1)}{1 - \nu^2} \begin{bmatrix} 1 & \nu & 0 \\ \nu & 1 & 0 \\ 0 & 0 & (1 - \nu)/2 \end{bmatrix} \quad (24b)$$

$$\{\Delta\varepsilon_i(t)\} = \frac{[1 - \lambda(t, t_1, t_o)]}{\bar{E}_{cs}(t, t_1)} \begin{bmatrix} 1 & -\nu & 0 \\ -\nu & 1 & 0 \\ 0 & 0 & 2(1 + \nu) \end{bmatrix} \begin{Bmatrix} \sigma_x(t_1) \\ \sigma_y(t_1) \\ \tau_{xy}(t_1) \end{Bmatrix} \quad (24c)$$

where the other vectors are the same as those in Section 3. Eq. (24a) is similar in form to Eq. (6a) but the important difference lies in the computational efficiency. Eq. (6a) requires SBSTI to calculate the stresses at the end of a stage whereas Eq. (24a) is capable of predicting the stresses in one step. The element stiffness matrix  $\mathbf{K}_{cs}$  can be written similar to Eq. (8) as

$$\mathbf{K}_{cs} = T\mathbf{A}\mathbf{B}^T \bar{\mathbf{D}}_{cs}(t)\mathbf{B} \quad (25)$$

Explicit forms of the stiffness matrix are given in Appendix A.

### 4.4. Bar elements using SAEM

Consider the bar element shown in Fig. 1(b) again and the variables defined in Section 3. Noting the incremental stress  $\Delta\sigma_c(t) = -\Delta F_1/A_b = \Delta F_2/A_b$  and the incremental strain  $\Delta\varepsilon_c(t) = (\Delta u_2 - \Delta u_1)/l$  in terms of the nodal quantities, Eq. (23a) can be used to formulate the incremental nodal force vector as

$$\begin{Bmatrix} \Delta F_1 \\ \Delta F_2 \end{Bmatrix} = \frac{\bar{E}_{cs}(t, t_1) A_b}{l} \begin{bmatrix} 1 & -1 \\ -1 & 1 \end{bmatrix} \begin{Bmatrix} \Delta u_1 \\ \Delta u_2 \end{Bmatrix} + [1 - \lambda(t, t_1, t_o)] \sigma_c(t_1) A_b \begin{Bmatrix} 1 \\ -1 \end{Bmatrix} + \bar{E}_{cs}(t, t_1) A_b \Delta \varepsilon_{cs}(t) \begin{Bmatrix} 1 \\ -1 \end{Bmatrix} \quad (26)$$

On the right hand side of Eq. (26), the first term accounts for the effect of incremental nodal displacements. The second term gives the effect of the initial stress at the stage considered while the last term describes the effect of shrinkage that has occurred at this stage.

## 5. Numerical examples

In the following numerical examples, the stresses and strains of concrete floors are determined by finite element analysis using SBSTI and SAEM for comparison in terms of efficiency, simplicity of use, computation time and accuracy of the results. The SBSTI solutions can be taken as reference solutions provided that the number of time steps is large enough to ensure convergence. Unless otherwise stated, uniform 1-day time intervals are used with the SBSTI method for simplicity although it is known that the use of increasing time intervals is more efficient. The CEB-FIP Model Code for Concrete structures 1990 (Comité Euro-International du Béton 1993) is used to obtain the concrete parameters.

### 5.1. Example 1: A square concrete slab restrained at two opposite sides

A square concrete slab of sides  $L = 10000$  mm and notional thickness  $h_o = 200$  mm is restrained at two opposite sides in such a way that movement along these edges is allowed but movement normal to them is not allowed. Curing is provided for 3 days after which shrinkage may occur. Analysis is carried out for the period from  $t_o = 3$  days to  $t_n = 365$  days using equal time steps. The slab is analysed by both two-dimensional and one-dimensional models. Fig. 4(a) shows a two-dimensional model comprising 32 triangular plane stress elements with a symmetrical mesh, while Fig. 4(b) shows a one-dimensional model. The problem is solved by both the SBSTI and SAEM methods using up to 1000 equal time steps to study the convergence of solution. Note that in the SAEM method, iterations in the time domain are only carried out for a single bar element to

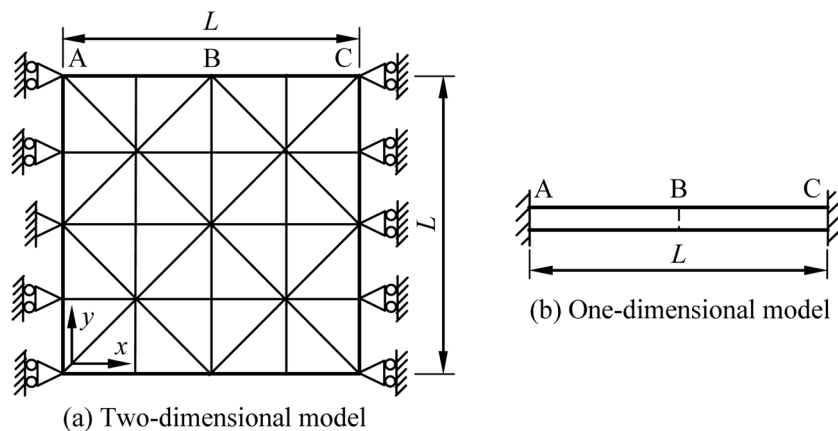


Fig. 4 Example 1: A square concrete slab restrained at two opposite sides

Table 1 Example 1: Convergence of stress  $\sigma_x$  at 365 days based on uniform time steps

Number of time steps	One-dimensional model		Two-dimensional model	
	SBSTI method (MPa)	SAEM method (MPa)	SBSTI method (MPa)	SAEM method (MPa)
3	2.608	2.608	2.608	2.608
5	2.589	2.589	2.589	2.589
10	2.540	2.540	2.540	2.540
50	2.420	2.420	2.420	2.420
100	2.385	2.385	2.385	2.385
200	2.359	2.359	2.359	2.359
500	2.336	2.336	2.335	2.335
1000	2.323	2.323	2.323	2.323

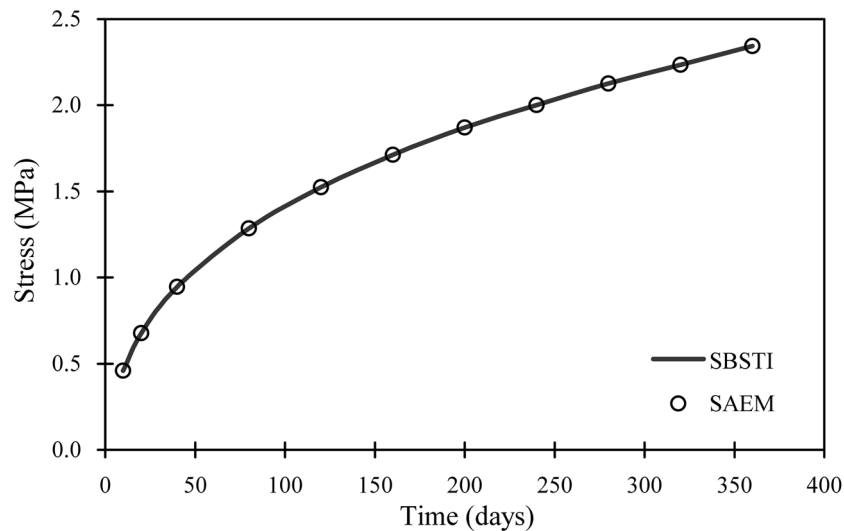


Fig. 5 Example 1: development of stress  $\sigma_x$  in slab cast in one stage

establish the SAEM and then the results at any time  $t$  can be solved in just one step. In this particular case, the stresses are uniformly distributed in the slab. The convergence of stresses  $\sigma_x$  in the  $x$ -direction at 365 days is shown in Table 1. It can be seen that excellent agreement is obtained. Therefore if the SAEM method is used, very fine time steps may be used to get accurate results with virtually no adverse effect on the computation time and memory requirement. Fig. 5 shows the development of stresses  $\sigma_x$  in the  $x$ -direction with time again indicating excellent agreement between the SAEM and SBSTI methods.

5.2. Example 2: A square concrete slab restrained at all sides and cast in a single stage

A square concrete slab restrained at all sides and cast in a single stage is considered. Its properties are the same as those in Example 1 except that here all sides are restrained. Fig. 6 shows a two-dimensional model for analysis. Equal time steps of  $\Delta t = 1$  day are adopted in the analysis for the

period from  $t_o = 3$  days to  $t_n = 365$  days. Because of symmetry, all elements have the same stresses, and the stresses along  $x$ - and  $y$ -axes are the same. Both the SAEM and SBSTI methods give the same results, namely  $\sigma_x = \sigma_y = 2.857\text{MPa}$  and  $\tau_{xy} = 0.000\text{MPa}$ , with no discrepancy. Excellent agreement is again observed.

### 5.3. Example 3: A square concrete slab restrained at all sides and cast in two stages

The square concrete slab restrained at all sides considered in this example is similar to that in Example 2 except that it is cast in two stages. The left half of the slab as shown shaded in Fig. 6 is cast at Day 0 and curing is provided for 3 days, while the right half is cast at Day 120 and curing is also provided to this portion for 3 days. For the sake of analysis, the two stages may be further split into four sub-stages. At Stage 1a (Days 0 to 3), no shrinkage in the left half is assumed to occur as it is still being cured. At Stage 1b (Days 3 to 120), shrinkage occurs in the left half which is restrained on three sides only. After casting the second half, no shrinkage occurs to the right half at Stage 2a (Day 120 to Day 123) but the continuing shrinkage of the left half tends to deform the right half. At Stage 2b (Days 123 to 365), the shrinkage of both halves acts together.

The problem is solved by both the SBSTI and SAEM methods using the two-dimensional model. Table 2 compares the stresses of selected elements obtained from the two methods. The maximum absolute error compared with the reference solution of  $12.0 \times 10^{-3}$  MPa (Element b) is considered acceptable in most engineering applications. In most cases, the percentage errors are below 0.5%.

### 5.4. Example 4: A typical podium structure cast in one stage

The simplified model of a typical rectangular podium structure of size 42 m $\times$ 90 m with two residential blocks as shown in Fig. 7 is studied. The podium structure is supported by two 10 m $\times$ 10 m core walls and 24 columns. As the core walls are generally very stiff, the nodes on the wall segments are taken to be fixed along both  $x$ - and  $y$ -axes. The columns are assumed to be restrained at both ends against rotation. Therefore the lateral stiffness of a column is  $12E_{col}I_{col}/L_{col}^3$  where  $E_{col}$

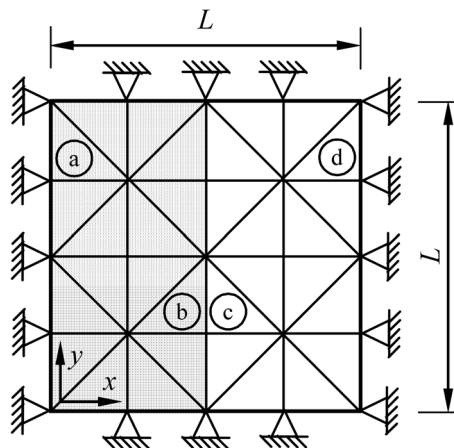


Fig. 6 Example 2 and 3: A square concrete slab restrained at all sides

Table 2 Example 3: Stresses of selected elements at the end of 365 days from two-dimensional model

Element	SBSTI method (MPa)			SAEM method (MPa)			Absolute error ( $10^{-3}$ MPa)			Percentage error (%)		
	$\sigma_x$	$\sigma_y$	$\tau_{xy}$	$\sigma_x$	$\sigma_y$	$\tau_{xy}$						
a	2.335	2.764	0.050	2.327	2.761	0.050	8	3	0	0.3	0.1	0.0
b	2.145	2.445	0.011	2.133	2.440	0.011	12	5	0	0.5	0.2	0.0
c	2.129	2.419	0.037	2.118	2.415	0.037	11	4	0	0.5	0.2	0.0
d	2.201	2.419	-0.034	2.194	2.417	-0.034	7	2	0	0.3	0.1	0.0

is the elasticity of mature concrete,  $I_{col}$  is an appropriate second moment of area and  $L_{col}$  is the length of column. The characteristic cube strength of concrete in the beams and slabs is 30 MPa while that of the columns and walls is 40MPa. The beams have the same cross sectional area of 500,000 mm<sup>2</sup> with steel reinforcement content of 0.4%. The slabs are 200 mm thick with 0.13% steel reinforcement along the  $x$ - and  $y$ -axes. The columns have the same cross section of 800 mm×800 mm and the walls are 200 mm thick. The concrete in the columns and walls are taken to be mature when the floor is cast and so the support stiffnesses are assumed to be independent of time. The slabs are modelled by triangular plane stress elements while the beams are modelled by bar elements. The column stiffnesses are assumed to be concentrated at the nodes for simplicity. Both the SBSTI and SAEM methods are used to solve the problem. The concrete stresses obtained are then compared to the tensile strength capacity to predict if cracking may occur.

Figs. 8 and 9 show the areas identified to be prone to cracking at the end of 365 days as shaded based on the tensile strength criteria of concrete by the SBSTI and SAEM methods respectively. It is observed that the results agree well with each other. Both methods indicate that tensile stresses are induced near the stiff core walls and they tend to spread to the area between the core walls. Certain areas in the vicinity of the columns are also predicted to be prone to cracking. Note that as both the structure and the mesh used are doubly symmetric, the results obtained are also doubly symmetric.

Two elements in the floor are chosen to further study the variation of stresses. Element No. 2395 is located in the vicinity of the segment of the left core wall facing the right one, while Element No. 3739 is located at the middle of the podium, as shown in Fig. 7. The comparisons of stresses and

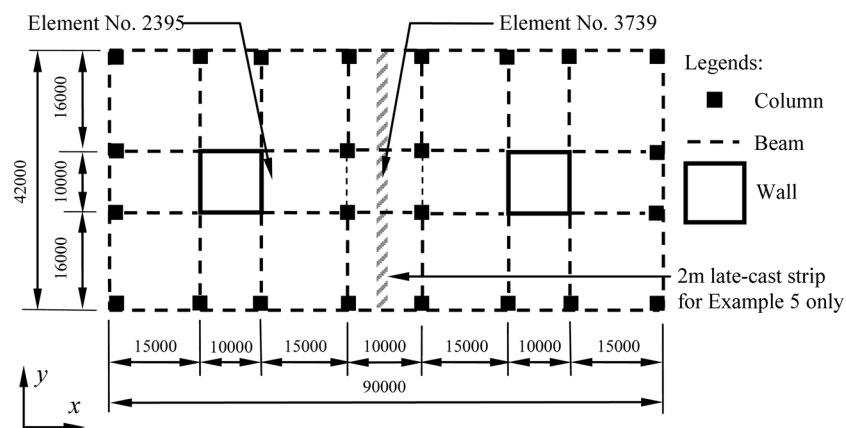


Fig. 7 Example 4 and 5: A simplified rectangular podium with two blocks

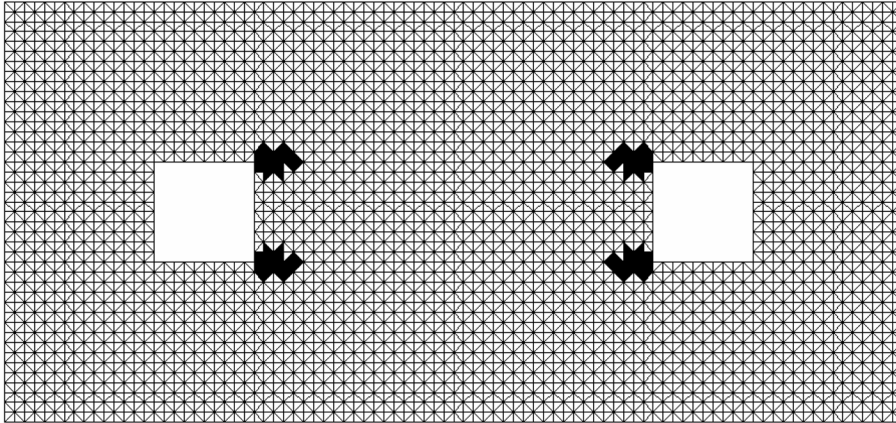


Fig. 8 Example 4: Areas predicted by the SBSTI method to be prone to cracking at the end of 365 days

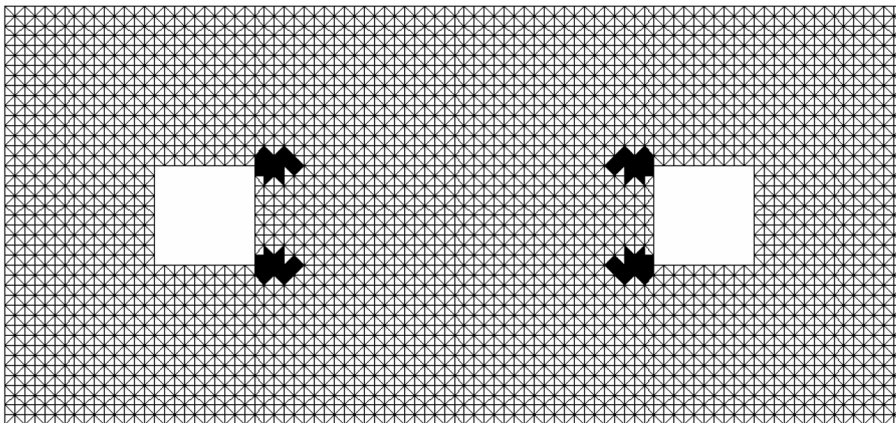


Fig. 9 Example 4: Areas predicted by the SAEM method to be prone to cracking at the end of 365 days

strains as shown in Tables 3 and 4 respectively indicate very good agreement. The principal stresses, principal strains and their orientations obtained by both methods are also in good agreement. Furthermore, Fig. 10 shows the variation of principal stresses with times for these two elements. Good agreement is again observed between the SBSTI and SAEM methods.

### 5.5. Example 5: A typical podium structure cast in two stages

The podium considered in this example is the same as that in Example 4 except that it is cast in two stages. Fig. 7 shows that most of the podium (first-cast area) is cast at Day 0 except for the shaded late-cast strip. Before casting the stitch, the two halves are relatively free to shrink with each centre of core wall as the effective point of fixity because the columns are much more flexible compared with the core walls. At Day 60, the late-cast strip is cast, and 3-day curing is provided to it. For the sake of analysis, the two stages may be further split into four sub-stages. At Stage 1a (Day 0 to Day 3), no shrinkage in the first-cast area occurs as it is still being cured. At Stage 1b (Day 3 to Day 60), shrinkage occurs in the first-cast area. At Stage 2a (Day 60 to Day 63) when the

Table 3 Example 4: Comparison of stresses at selected positions

Element No.	SBSTI method (MPa)			SAEM method (MPa)			Absolute error (MPa)		
	$\sigma_x$	$\sigma_y$	$\tau_{xy}$	$\sigma_x$	$\sigma_y$	$\tau_{xy}$			
2395	1.21	0.87	-0.17	1.22	0.86	-0.17	-0.01	0.01	0.00
3739	2.39	0.39	0.00	2.40	0.39	0.00	-0.01	0.00	0.00
	Principal stress (MPa) and orientation			Principal stress (MPa) and orientation			Absolute error (MPa)		
2395	1.28 (22.2°)			1.29 (22.2°)			-0.01		
3739	2.39 (0.0°)			2.40 (0.0°)			-0.01		

Table 4 Example 4: Comparison of strains at selected positions

Element No.	SBSTI method ( $\times 10^{-6}$ )			SAEM method ( $\times 10^{-6}$ )			Absolute error ( $\times 10^{-6}$ )		
	$\epsilon_x$	$\epsilon_y$	$\gamma_{xy}$	$\epsilon_x$	$\epsilon_y$	$\gamma_{xy}$			
2395	-82.8	-108.8	-24.9	-82.9	-108.2	-24.8	0.1	-0.6	-0.1
3739	-3.5	-152.6	0.0	-3.6	-151.9	0.0	0.1	-0.7	0.0
	Principal strain ( $\times 10^{-6}$ ) and orientation			Principal strain ( $\times 10^{-6}$ ) and orientation			Absolute error ( $\times 10^{-6}$ )		
2395	-113.8 (-31.2°)			-113.3 (-31.5°)			-0.5		
3739	-152.5 (0.0°)			-151.9 (0.0°)			-0.6		

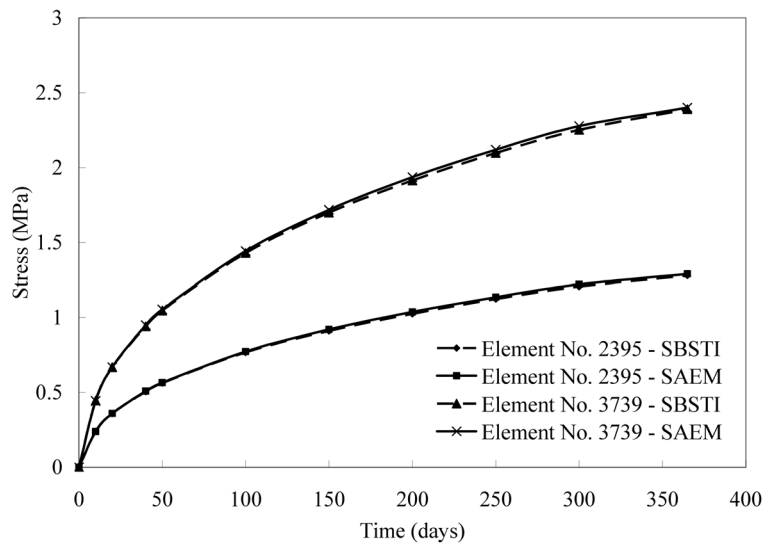


Fig. 10 Example 4: Variation of principal stresses at Element Nos. 2395 and 3739 predicted by the SBSTI and SAEM methods

late-cast strip is being cured, no shrinkage occurs to it but the continuing shrinkage of the first cast portions tends to deform the late-cast strip. At Stage 2b (Day 63 to Day 365), the shrinkage of the whole podium acts together.

Figs. 11 and 12 show the areas identified to be prone to cracking at the end of 365 days as shaded

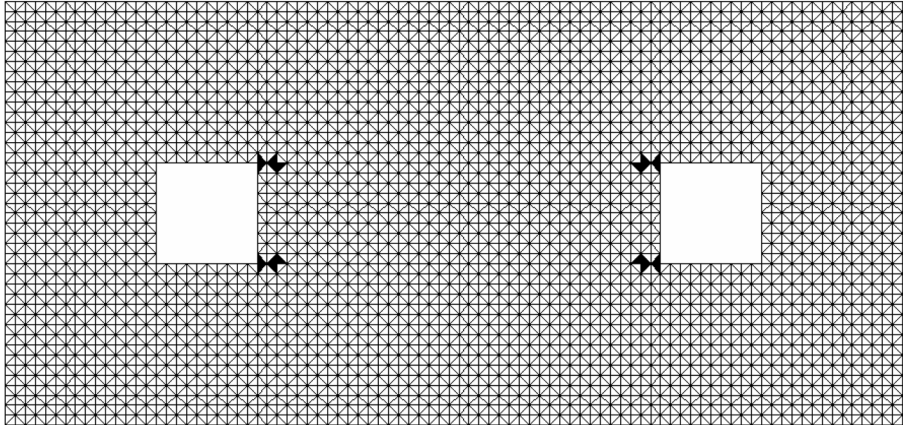


Fig. 11 Example 5: Areas predicted by the SBSTI method to be prone to cracking at the end of 365 days

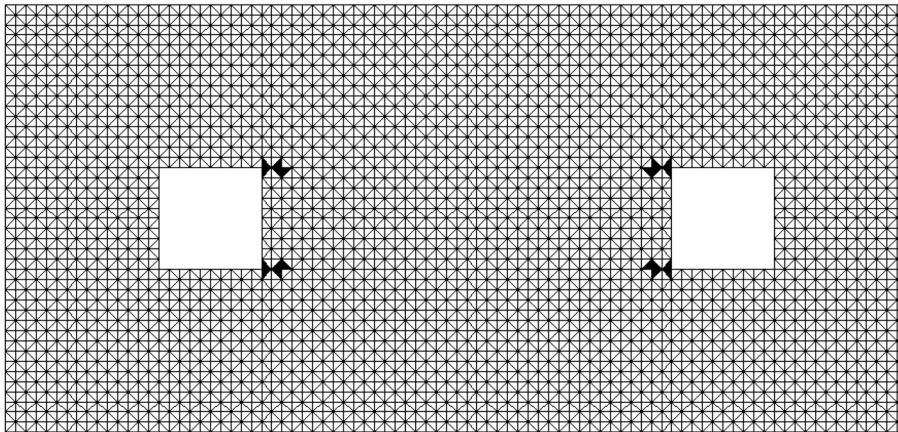


Fig. 12 Example 5: Areas predicted by the SAEM method to be prone to cracking at the end of 365 days

based on the tensile strength criteria of concrete by the SBSTI and SAEM methods respectively. It is observed that the results agree well with each other. Compared with Example 4, the tensile cracking problem is alleviated. Fig. 13 shows the variation of principal stresses with time for the same two elements selected in Example 4. The comparisons of stresses and strains as shown in Tables 5 and 6 respectively indicate very good agreement between the two models.

### 5.6. Computational efficiency

Table 7 shows the computation time spent on the above-mentioned examples. The advantage of the SAEM method is obvious especially for large problems such as the podium structure in Examples 4 and 5. For the SBSTI method, the finite element computation requires 362 steps. It can be seen that the computation time of the SAEM method is much less because it involves one step only. Therefore the SAEM method is particularly suitable for large problems.

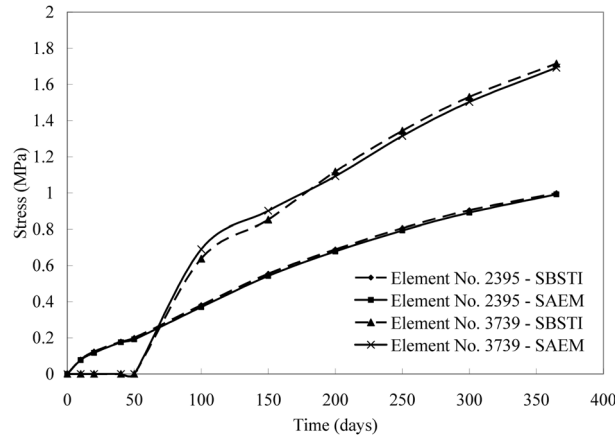


Fig. 13 Example 5: Variation of principal stresses at Element Nos. 2395 and 3739 predicted by the SBSTI and SAEM methods

Table 5 Example 5: Comparison of stresses at selected positions

Element No.	SBSTI method (MPa)			SAEM method (MPa)			Absolute error (MPa)		
	$\sigma_x$	$\sigma_y$	$\tau_{xy}$	$\sigma_x$	$\sigma_y$	$\tau_{xy}$			
2395	0.93	0.78	-0.13	0.92	0.76	-0.12	0.01	0.02	-0.01
3739	1.72	1.00	0.00	1.70	1.23	0.00	0.02	-0.23	0.00
	Principal stress (MPa) and orientation			Principal stress (MPa) and orientation			Absolute error (MPa)		
2395	1.00(-29.6°)			0.99 (-28.6°)			0.01		
3739	1.72 (0.0°)			1.70 (0.0°)			0.02		

Table 6 Example 5: Comparison of strains at selected positions

Element No.	SBSTI method ( $\times 10^{-6}$ )			SAEM method ( $\times 10^{-6}$ )			Absolute error ( $\times 10^{-6}$ )		
	$\epsilon_x$	$\epsilon_y$	$\gamma_{xy}$	$\epsilon_x$	$\epsilon_y$	$\gamma_{xy}$			
2395	-108.8	-114.3	-15.3	-108.6	-113.9	-15.3	-0.2	-0.4	0.0
3739	1358.5	-149.3	1.2	1349.3	-148.3	1.1	9.2	-1.0	0.1
	Principal strain ( $\times 10^{-6}$ ) and orientation			Principal strain ( $\times 10^{-6}$ ) and orientation			Absolute error ( $\times 10^{-6}$ )		
2395	-119.7 (-39.8°)			-119.4 (-40.1°)			-0.3		
3739	-149.4 (0.0°)			-148.3(0.0°)			-1.1		

Table 7 Comparison of computation time of the SBSTI and SAEM methods

Example	SBSTI method (s)	SAEM method (s)
1	5.468	0.00156
2	5.468	0.00156
3	5.578	0.00156
4 and 5	1861.4	5.468

## 6. Conclusions

To overcome the difficulties associated with the shrinkage movement analysis using the SBSTI method, the SAEM method is introduced. The SAEM may be easily worked out by considering a single bar element of concrete. Afterwards the deformations of the whole structure can be analysed by finite element method using one single step. It drastically cuts down the computation time needed for shrinkage movement analysis. The SAEM can be used to derive the shrinkage-adjusted relaxation function which enables the method to cope with restraints introduced at any time after casting. Therefore floors cast in several stages can also be analysed by this method. Numerical examples of different sophistication are presented to demonstrate the usefulness of the SAEM method. To certain extent, the SAEM method makes it possible to separate the discretisation in time domain from the discretisation of geometry. Very fine time steps may be used to derive the SAEM and shrinkage-adjusted relaxation function using just a single bar element of concrete. These values can then be applied to a fine geometric mesh using just one big time step. The SAEM method presents a convenient way for prediction of the general onset of cracking and provides important clues to refinements in the preliminary design to avoid subsequent shrinkage problems.

## Acknowledgement

The work described in this paper has been partially supported by the Committee on Research and Conference Grants, The University of Hong Kong, Hong Kong.

## References

- Alexander, S. (2002a), "Understanding shrinkage and its effects: Part 1", *Concrete*, **36**(9), 61-63.
- Alexander, S. (2002b), "Understanding shrinkage and its effects: Part 2", *Concrete*, **36**(10), 38-41.
- Altoubat, S.A. and Lange, D.A. (2001), "Creep, shrinkage, and cracking of restrained concrete at early age", *ACI Mater. J.*, **98**(4), 323-331.
- Au, F. T. K., Liu, C. H. and Lee, P. K. K. (2007), "Creep and shrinkage analysis of reinforced concrete frames by history-adjusted and shrinkage-adjusted elasticity moduli", *The Structural Design of Tall and Special Buildings* (to appear).
- Bazant, Z. P. (1972), "Prediction of concrete creep effects using age-adjusted effective modulus method", *ACI J.*, **69**(4), 212-219.
- Bazant, Z. P. (1982), "Mathematical models for creep and shrinkage of concrete", *Creep and Shrinkage in Concrete Structure*, John Wiley and Sons, New York, 163-256.
- Bazant, Z. P. (1988), "Material models for structural creep analysis", *Mathematical Modeling of Creep and Shrinkage of Concrete*, John Wiley and Sons, New York, 99-215.
- Bazant, Z. P. (2001), "Prediction of concrete creep and shrinkage: Past, present and future", *Nuclear Eng. Design*, **203**(1), 27-38.
- Comité Euro-International du Béton (1993), CEB-FIP Model Code for Concrete Structures (MC-90), Paris-London-Berlin.
- Cheung, Y. K. and Au, F. T. K. (1992), "Finite strip analysis of right box girder bridges using computed shape functions", *Thin-Walled Struct.*, **13**(4), 275-298.
- Cheung, Y. K. and Yeo, M. F. (1979), *A Practical Introduction to Finite Element Analysis*. Pitman, London.
- Cook, R. D., Malkus, D. S. and Plesha, M. E. (2002), *Concepts and Applications of Finite Element Analysis*, 4<sup>th</sup> Ed., John Wiley & Sons Press, New York.

- Dilger, W. H. and Neville, A. M. (1971), "A method of creep analysis of structural members", *Designing for Effects of Creep Shrinkage Temperature in Concrete Structures*, ACI Special Publication No. 27, 349-371.
- Ghali, A., Favre, R. and Elbadry, M. (2002), *Concrete Structures: Stresses and Deformations*, 3<sup>rd</sup> Ed., Spon Press, London.
- Gilbert, R. I. (1988), *Time Effects in Concrete Structures*, Amsterdam: Elsevier Science Publishers.
- Gilbert, R. I. (1992), "Shrinkage cracking in fully-restrained concrete members", *ACI Struct. J.* **101**(6), 840-845.
- Kim, H. S. and Cho, S. H. (2004), "Shrinkage stress analysis of concrete slabs with shrinkage strips in a multistorey building", *Comput. Struct.*, **82**(15-16), 1143-1152.
- Kim, H. and Cho, S. (2005), "Shrinkage stress analysis of concrete slab in multistorey building considering variation of restraint and stress relaxation due to creep", *Structural Design of Tall and Special Buildings*, **14**(1), 47-58.
- Liu, C. H., Au, F. T. K. and Lee, P. K. K. (2006), "Estimation of shrinkage effects on reinforced concrete podiums", *HKIE Transactions*, **13**(4), 33-43.
- Nejadi, S. and Gilbert, I. (2004), "Shrinkage cracking and crack control in restrained reinforced concrete members" *ACI Struct. J.*, **101**(6), 840-845.
- Trost, H. (1967), "Auswirkungen des Superpositionsprinzips auf Kriech- und Relaxation- Probleme bei Beton und Spannbeton", *Beton- und Stahlbetonbau*, **62**(10), 230-238 and **62**(11), 261-269.

## Appendix A: Finite element analysis of the RC floors by triangular plane stress element

The incremental displacement vector is  $\Delta\delta = [u_i, v_i, u_j, v_j, u_m, v_m]^T$  where  $u_i$  and  $v_i$  are displacements of node  $i$  in the  $x$ - and  $y$ -directions respectively. The incremental load vector is  $\Delta\mathbf{q}^e = [F_{ix}, F_{iy}, F_{jx}, F_{jy}, F_{mx}, F_{my}]^T$  where  $F_{ix}$  and  $F_{iy}$  are nodal forces at node  $i$  in the  $x$ - and  $y$ -directions respectively. The strain matrix is

$$\mathbf{B} = \frac{1}{2A} \begin{bmatrix} b_i & 0 & b_j & 0 & b_m & 0 \\ 0 & c_i & 0 & c_j & 0 & c_m \\ c_i & b_i & c_j & b_j & c_m & b_m \end{bmatrix}$$

where  $b_i = y_i - y_m$ ,  $b_j = y_m - y_i$ ,  $b_m = y_i - y_j$ ,  $c_i = x_m - x_j$ ,  $c_j = x_i - x_m$ ,  $c_m = x_j - x_i$  and  $A$  is the area of triangular element with nodes  $i, j$  and  $m$ .

The stiffness matrices for step-by-step time integration and shrinkage-adjusted elasticity modulus are similar except for a few parameters. The stiffness matrix for step-by-step time integration is

$$\mathbf{K}_c = \frac{T}{4A} \begin{bmatrix} K_{11} & K_{12} & K_{13} & K_{14} & K_{15} & K_{16} \\ K_{21} & K_{22} & K_{23} & K_{24} & K_{25} & K_{26} \\ K_{31} & K_{32} & K_{33} & K_{34} & K_{35} & K_{36} \\ K_{41} & K_{42} & K_{43} & K_{44} & K_{45} & K_{46} \\ K_{51} & K_{52} & K_{53} & K_{54} & K_{55} & K_{56} \\ K_{61} & K_{62} & K_{63} & K_{64} & K_{65} & K_{66} \end{bmatrix}$$

with parameters  $c_1 = \frac{\bar{E}_{cs}(t, t_1)}{1 - \nu^2}$ ,  $c_2 = \nu$ , and  $c_{12} = \frac{c_1(1 - c_2)}{2}$ .

The stiffness matrix for shrinkage-adjusted elasticity modulus is

$$\mathbf{K}_{cs} = \frac{T}{4A} \begin{bmatrix} K_{11} & K_{12} & K_{13} & K_{14} & K_{15} & K_{16} \\ K_{21} & K_{22} & K_{23} & K_{24} & K_{25} & K_{26} \\ K_{31} & K_{32} & K_{33} & K_{34} & K_{35} & K_{36} \\ K_{41} & K_{42} & K_{43} & K_{44} & K_{45} & K_{46} \\ K_{51} & K_{52} & K_{53} & K_{54} & K_{55} & K_{56} \\ K_{61} & K_{62} & K_{63} & K_{64} & K_{65} & K_{66} \end{bmatrix}$$

with parameters  $c_1 = \frac{\bar{E}_c(t, t_1)}{1 - \nu^2}$ ,  $c_2 = \nu$  and  $c_{12} = \frac{c_1(1 - c_2)}{2}$ . Both matrices are symmetrical, i.e.  $K_{ij} = K_{ji}$  and the coefficients on or above the main diagonal are as follows:

$$K_{11} = c_1 b_i^2 + c_{12} c_i^2$$

$$K_{12} = (c_1 c_2 + c_{12}) b_i c_i$$

$$K_{13} = c_1 b_j b_j + c_{12} c_i c_j$$

$$K_{14} = c_1 c_2 b_i c_j + c_{12} b_j c_i$$

$$K_{15} = c_1 b_i b_m + c_{12} c_i c_m$$

$$K_{16} = c_1 c_2 b_i c_m + c_{12} b_m c_i$$

$$K_{22} = c_1 c_i^2 + c_{12} b_i^2$$

$$K_{23} = c_1 c_2 b_j c_i + c_{12} b_i c_j$$

$$K_{24} = c_1 c_i c_j + c_{12} b_i b_j$$

$$K_{25} = c_1 c_2 b_m c_i + c_{12} b_i c_m$$

$$K_{26} = c_1 c_i c_m + c_{12} b_i b_m$$

$$K_{33} = c_1 c_j^2 + c_{12} c_j^2$$

$$K_{34} = (c_1 c_2 + c_{12}) b_j c_j$$

$$K_{35} = c_1 b_j b_m + c_{12} c_j c_m$$

$$K_{36} = c_1 c_2 b_j c_m + c_{12} b_m c_j$$

$$K_{44} = c_1 c_j^2 + c_{12} b_j^2$$

$$K_{45} = c_1 c_2 b_m c_j + c_{12} b_j b_m$$

$$K_{46} = c_1 c_j c_m + c_{12} b_j b_m$$

$$K_{55} = c_1 b_m^2 + c_{12} c_m^2$$

$$K_{56} = (c_1 c_2 + c_{12}) b_m c_m$$

$$K_{66} = c_1 c_m^2 + c_{12} b_m^2$$

CC